High-Quality Ultralong Sb_2S_3 Nanoribbons on Large Scale

Y. Yu,[†] R. H. Wang,[†] Q. Chen,[‡] and L.-M. Peng*[,†,‡]

Beijing Laboratory of Electron Microscopy, Institute of Physics, Chinese Academy of Science, Beijing 100080, China, and Key Laboratory on the Physics and Chemistry of Nanodevices and Department of Electronics, Peking University, Bejing 100871, China

Received: September 11, 2005; In Final Form: October 17, 2005

Large-scale, ultralong, single-crystalline Sb_2S_3 nanoribbons were prepared by directly reacting $SbCl_3$ and $Na_2S_2O_3$ solutions, without any organics used in the experiment. The nanoribbons were analyzed by a range of methods. The nanoribbons are usually several millimeters in length, typically 200−500 nm in width and 30−80 nm in thickness. The structure of the nanoribbons is determined to be of the orthorhombic phase. The growth mechanism of the nanoribbons was investigated based on high-resolution transmission electron microscopy observations. Optical absorption experiment shows that the nanoribbon is a semiconductor with a bandwidth $E_g \approx 1.5$ eV, near to the optimum for photovoltaic conversion, suggesting that Sb_2S_3 nanoribbons could be used in solar energy and photoelectronic applications.

1. Introduction

One-dimensional semiconductor nanomaterials, such as nanotubes, nanowires, and nanoribbons have attracted considerable interest for scientific research in recent years, because of their remarkable electronic, magnetic, optical, catalytic, and mechanical properties which are different from that of the bulk materials, and these nanomaterials may eventually lead to applications in nanodevices.[1−3] Among these materials, antimony trisulfide is a typical binary compound with a crystal structure belonging to the orthorhombic system and a space group D_{2h}^{16}.[4,5] It consists of a layer-like $(Sb_4S_6)_n$ polymer linked together by intermolecular attraction between antimony and sulfur atoms. The bonds within the layers are different in length owing to the two different types of coordination exhibited by both antimony and sulfur. Sb_2S_3 is an important semiconductor with high photosensitivity and thermoelectric power.[6] Sb_2S_3 is regarded as a prospective material for solar energy due to its good photoconductivity.[7] It has also been used in thermoelectric cooling technology and photoelectronics in the IR region.[8,9] The principal semiconducting parameters of Sb_2S_3 crystals determined by different authors disagree strongly. The room temperature conductivity was reported to range from 10^{-6} to 10^{-10} Ω^{-1} cm^{-1}.[10,11] The reported values of the band gap of the Sb_2S_3 crystals, determined from optical measurement, are 1.55,[12] 1.64,[13] 0.9,[14] and 1.72 eV.[15] As a result of these disagreements on Sb_2S_3 crystals semiconducing parameters together with its good photoconductivity and useful photovoltaic properties, Sb_2S_3 has been attracting great research attention. Sb_2S_3 thin films[16−18] and one-dimensional materials, including nanorods[19−22] and nanotubes,[15,23] have been synthesized by various methods. The newly distinct one-dimensional nanostructures with ribbon-like or belt-like morphologies, which are promising for sensor applications due to the fact that the *S*/*V* is very high, have been successfully prepared for semiconducting metal oxides by evaporating the desired metal oxides powders at a high temperature.[24−26] A solution-phase approach (hydrothermal reaction) for preparing nanoribbons, which may provide a more promising method to nanoribbons than conventional methods in terms of cost and potential for large-scale production, has seldom been reported.[27,28] However, most hydrothermal reactions for one-dimensional nanomaterials need organics to assist the synthesis, which is harmful to the environment. Qian and co-workers have successfully prepared Bi_2S_3 nanoribbons using the organics-assisted solvothermal method.[28] To the best of our knowledge, the Sb_2S_3 nanoribbons have not been reported up to now. Herein, we report a simple hydrothermal method for synthesizing high-quality, single-crystal Sb_2S_3 nanoribbons with lengths of up to a few millimeters by reacting $SbCl_3$ and $Na_2S_2O_3$ in distilled water, without any organics used in the synthesis process. The structure, growth mechanism, and optical absorption at room temperature of the Sb_2S_3 nanoribbons were investigated.

2. Experimental Section

All of the chemical reagents used in this experiment were analytical grade. In a typical experimental, 0.0025 mol $SbCl_3$ was first added into 60 mL distilled water, to produce white precipitates. After stirring for 15 min, 0.003 75 mol $Na_2S_2O_3$ was introduced and continued to stir for 30 min; the white precipitates were turning into orange precipitates. The mixed solution was then transferred into a Teflon-lined stainless steel autoclave (80 mL capacity), sealed, and maintained at 180 °C for 3 days. After the reaction, the resulting black solid product was filtered and washed with distilled water to remove ions remaining in the products. The final products were then dried in air.

The powder X-ray diffraction (XRD) experiment was performed with a Rigaku D/max 2400 diffractometer using monochromatic Cu Kα radiation ($\lambda = 1.54$ Å) under 40 kV and 120 mA and scanning between 5° and 70° (2θ). Transmission electron microscopy (TEM) studies were performed using a 200 keV TEM Tecnai 20 and a field-emission gun TEM CM200/FEG. Scanning electron microscopy (SEM) was carried out using a field-emission gun SEM (FESEM) XL30 S-FEG

* To whom correspondence should be addressed. E-mail: lmpeng@pku.edu.cn.
[†] Chinese Academy of Science.
[‡] Peking University.

10.1021/jp055132z CCC: $30.25
Published on Web 11/17/2005

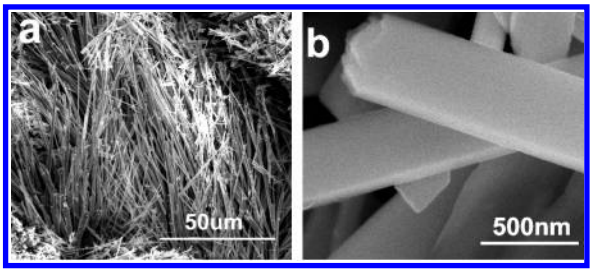

Figure 1. FESEM images of the as-synthesized Sb_2S_3 nanoribbons. (a) Low magnification FESEM image of the products showing that the product contains a large quantity of wirelike materials. (b) High magnification FESEM image showing two nanoribbons with rectangular cross sections which are about 65 nm in thickness and 350 and 400 nm in width, respectively.

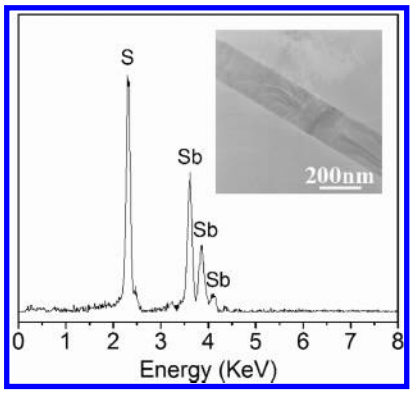

Figure 2. EDX spectrum taken from a single nanoribbon giving the nanoribbons a possible composition of Sb_2S_3. The inset shows the nanoribbon used in the EDX experiment.

(FEI SIRION). Composition of the specimens was analyzed using energy-dispersive X-ray spectroscopy (EDX) attached to the Tecnai 20. The specimens for TEM studies were prepared by dispersing the products in alcohol followed by ultrasonic treatment. The sample was then dropped onto a holey carbon film supported on a copper grid and dried in air. Band gap energy of the product was determined from the onset of the absorbance spectra of the sample on a UV−Vis−NIR spectrophotometer (Shimadzu UV-3100).

3. Results and Discussions

The morphologies of the product were determined with FESEM. Shown in Figure 1 are two FESEM images of the product taken with different magnifications. Figure 1a shows that the product contains a large quantity of wirelike materials. The lengths of the products ranged from tens of micrometers to a few millimeters. Closer inspection revealed that the geometrical shape of the 1D sample appears to be that of a nanoribbon structure. Figure 1b clearly displays the wide surface and the side surface of two nanoribbons. The two nanoribbons with rectangular cross sections are about 350 and 400 nm in width, respectively. Both their thicknesses are about 65 nm. Extensive TEM and FESEM observations reveal that the nanoribbons are typically 200−500 nm in width and 30−80 nm in thickness.

To determine the composition of the nanoribbons, EDX was performed on individual nanoribbons. Figure 2 is an EDX spectrum obtained from a single nanoribbon shown in the inset of Figure 2. Only Sb and S peaks are observed in this spectrum, suggesting that the nanoribbon is composed of mainly Sb and S. Quantitative EDX analysis shows that the atom ratio of Sb/S is 42:58, close to 2:3, giving the nanoribbons a possible composition of Sb_2S_3.

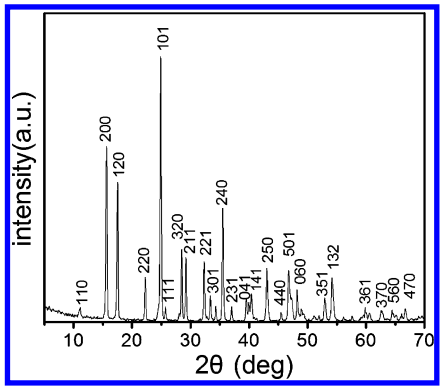

Figure 3. XRD profile recorded from the nanoribbon sample is well-indexed using the orthorhombic phase Sb_2S_3 (JCPDS 42-1393), suggesting the nanoribbon sample is a very high-purity, single-phase sample.

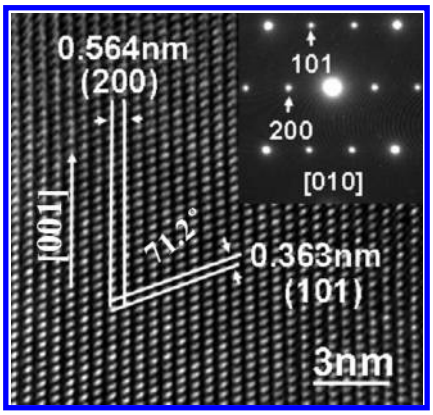

Figure 4. HRTEM image of a Sb_2S_3 nanoribbon, where the insert is the corresponding SAED pattern taken along the [010] zone axis.

X-ray powder diffraction (XRD) analysis was used to determine the structure of the nanoribbons. The results are shown in Figure 3. All the peaks in Figure 3 may well be indexed as the orthorhombic phase of Sb_2S_3 (cell constants: a = 11.23 Å, b = 11.31 Å, c = 3.841 Å; JCPDS 42-1393). No peaks of any other phases were detected, indicating that our nanoribbons sample is a very high-purity, single-phase sample.

The structure of nanoribbons is further investigated using high-resolution transmission electron microscopy (HRTEM) and electron diffraction (ED). A HRTEM image of a single Sb_2S_3 nanoribbon is shown in Figure 4, where the inset is the corresponding ED pattern, and as with the XRD profile, the HRTEM image and the ED pattern may also be indexed using the orthorhombic phase of Sb_2S_3 (JCPDS 42-1393). A further confirmation of the Sb_2S_3 nanoribbons structure was obtained. The lattice spacings of about 0.564 and 0.363 nm correspond to the (200) and (101) planes spacing of orthorhombic phase Sb_2S_3, respectively. The angle between the (200) and (101) planes is 71.2°. The ED pattern taken along [010] zone axis is a spot pattern, which reveals that the nanoribbon is single crystal in nature. Both the HRTEM image and the ED pattern demonstrate that the nanoribbon grows along [001] direction indicated with an arrow in Figure 4, which coincides with that previously reported for Sb_2S_3 nanorods.[19] Figure 4 also reveals that the nanoribbons quality is very high, free from dislocation and stacking faults.

To understand the growth mechanism, extensive TEM observations and EDX experiments were performed on samples with different hydrothermal reaction times, and the results are shown in Figure 5. In a typical experiment, $SbCl_3$ was first strongly hydrolyzed in water to produce white precipitates of

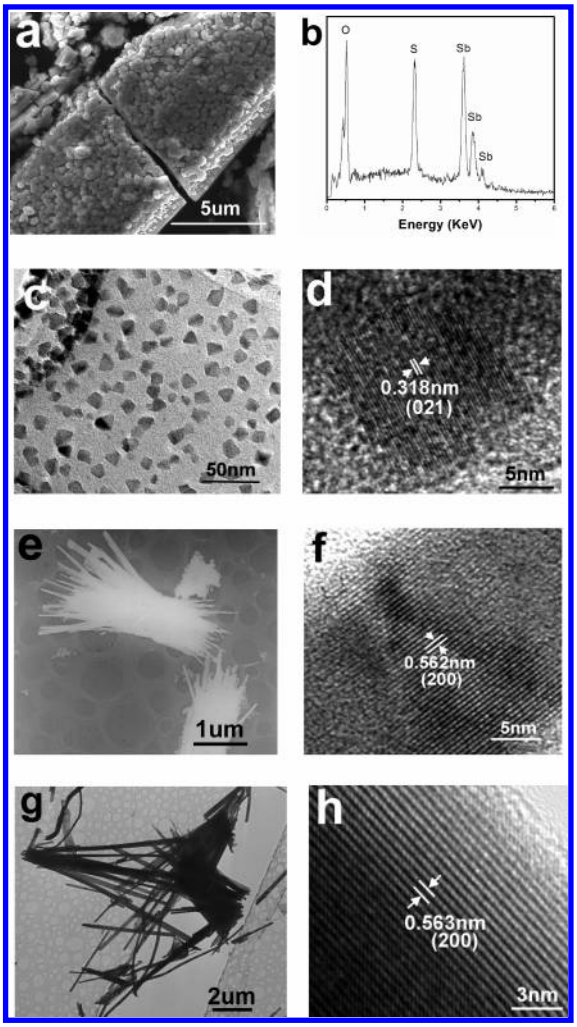

Figure 5. A series of experimental images showing the growth process of the nanoribbons. (a) A SEM image of the sample before hydrothermal reaction showing some orange particles grew out from the SbOCl surface. (b) A EDX spectrum taken from the orange particles, showing the orange particles are composed of mainly Sb, S, and O elements, giving a possible composition of $Sb_xS_yO_z$. (c) A TEM image showing many nanoparticles obtained by radiating a $Sb_xS_yO_z$ particle about 800 nm in diameter with an electron beam for 3 min. (d) A HRTEM image taken from one of these nanoparticles showing that these nanoparticles obtained from the decomposition of larger $Sb_xS_yO_z$ particles are indeed Sb_2S_3 particles. (e and f) TEM images show that short nanoribbons began to appear after reaction for 2 h. (g and h) TEM images show that these short nanoribbons became longer and better-crystallized after reaction for 6 h.

SbOCl. A TEM experiment reveals that the morphologies of SbOCl are some microparticles, 2−15 μm in diameter. An XRD experiment shows these microparticles are amorphous phases. Once $Na_2S_2O_3$ was introduced, orange precipitates were formed on the surface of the SbOCl microparticles. Figure 5a is a SEM image of the sample before hydrothermal reaction showing that some particles, more than 500 nm in diameter, pile up on the surface of the SbOCl microparticles. The transformation of the solution color (from white to orange) evidently results from these particles. XRD and ED experiments show these orange particles are also amorphous phases. Figure 5b is an EDX spectrum taken from these orange particles showing that only Sb, S, and O peaks are observed, suggesting that the orange particles are composed of mainly Sb, S, and O elements. Quantitative EDX analysis shows that the atom ratio of Sb/S/O is 28:34:38. Because of the existence of the O atom, the data of the atom ratio is not credible, which cannot give a real composition, giving a possible

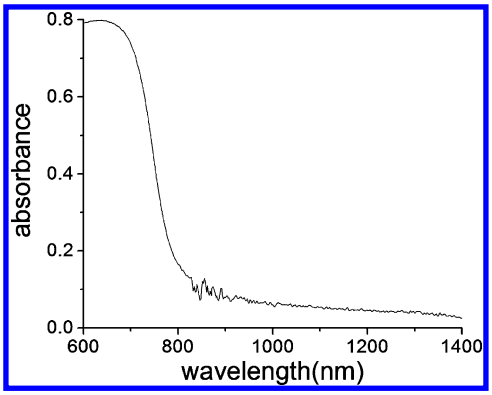

Figure 6. Experimental UV−visible spectrum obtained from Sb_2S_3 nanoribbons.

one of $Sb_xS_yO_z$. During our TEM observations, we found the compound of $Sb_xS_yO_z$ is very unstable under the radiation of electron beam. The $Sb_xS_yO_z$ easily decomposed under electron beam for short time. Figure 5c is a TEM image of the sample obtained by radiating at a $Sb_xS_yO_z$ particle about 800 nm in diameter with an electron beam for 3 min. The radiation of electron beam made the $Sb_xS_yO_z$ particles decompose into many nanoparticles about 8−12 nm in diameter. Figure 5d is a HRTEM image taken from one of these nanoparticles, showing lattice spacings that are the same as that of Sb_2S_3, verifying that these nanoparticles obtained from the decomposition of larger $Sb_xS_yO_z$ particles are indeed Sb_2S_3 particles. The experiment results revealed that $Sb_xS_yO_z$ is a kind of unstable compound that can decompose into Sb_2S_3 in some circumstance. Figure 5e is the TEM image of the sample after hydrothermal reaction for 2 h; many short nanoribbons formed about tens nanometers in width and hundreds of nanometers in length from mutual root part, which look like the growth mechanism of the potassium titanate nanowires induced by phase transformation.[29] The higher-magnification TEM image of a single short nanoribbon shown in Figure 5f shows that the structure of the short nanoribbons is the same as that of Sb_2S_3. An EDX experiment shows that Cl and O elements exist in the sample (hydrothermal reaction for 2 h), especially in the root part of the short nanoribbons, revealing that the short nanoribbons grew from the orange particles $Sb_xS_yO_z$ matrix on the SbOCl surface and the SbOCl continue to turn into $Sb_xS_yO_z$ during the growth process of the Sb_2S_3 nanoribbons. We therefore concluded that the Sb_2S_3 nanoribbons resulted from the simple decomposition of $Sb_xS_yO_z$ during the hydrothermal reaction. The decomposition of $Sb_xS_yO_z$ provide Sb_2S_3 nucleus, and the nucleus grows into Sb_2S_3 nanoribbons in the process of hydrothermal reaction. Figure 5f also reveals that the quality of these short nanoribbons is rather poor. They are not fully crystallized. Longer hydrothermal reaction times subsequently reduced the amorphous phase, giving much better quality nanoribbons. Shown in Figure 5g,h are similar TEM images for longer nanoribbons (several microns in lengths) obtained from the samples after 6 h of hydrothermal reaction. The nanoribbons shown in Figure 5g,h have a better quality than those shown in Figure 5e,f. An EDX experiment shows that O elements in modicum still exist in the root part of the nanoribbons, showing the growth process of the nanoribbons is not over. A Cl peak was hardly observed, suggesting that the SbOCl almost fully turns into $Sb_xS_yO_z$ in this stage (hydrothermal reaction for 6 h). On the basis of our experiments, we propose the growth process of Sb_2S_3 nanoribbons may contain three stages. First, $SbCl_3$ strongly hydrolyzed into SbOCl. Second, SbOCl reacted with $Na_2S_2O_3$ to produce orange $Sb_xS_yO_z$. Finally, $Sb_xS_yO_z$ decomposes into

Sb_2S_3 nanoparticles, and these Sb_2S_3 nanoparticles grow into Sb_2S_3 nanoribbons. Among the three stages, the second and the last stages simultaneously proceed in some time.

An optical absorption experiment was carried out to elucidate information on the band gap energy, which is one of the most important electronic parameters for semiconductor nanomaterials. Shown in Figure 6 is a typical UV−visible absorption spectrum of the Sb_2S_3 nanoribbons. Because all experimental works, including XRD, ED, EDX, and image observations revealing that the product is highly pure Sb_2S_3 nanoribbons, we expect the absorption spectrum represents the true absorption behavior of the Sb_2S_3 nanoribbons. The λ_{onset} of the spectrum recorded from the nanoribbons sample is about 800 nm. The band gap of the Sb_2S_3 nanoribbons may be estimated at 1.5 eV using the following formula:

$$\alpha = \sqrt{h\upsilon - E_g}/h\upsilon$$

where $h\upsilon$ is the corresponding phonon energy, α is absorbance, and this value lies at about the lower end of the values determined by other groups.[12−15] The fact that experimentally determined E_g varies from group to group suggests that it may depend on the details of the synthetic method employed and perhaps also on defect configurations. Our nanoribbons are about 65 nm × 400 nm in size, and we do not expect the corresponding E_g is very different from that of bulk materials. The experimentally determined E_g value of our Sb_2S_3 nanoribbons is near to the optimum for photovoltaic conversion,[10] which suggests that Sb_2S_3 nanoribbons may be very promising for applications in solar energy and photoelectronics.

4. Conclusion

High-quality ultrolong Sb_2S_3 nanoribbons with 200−500 nm in width and 30−80 nm in thickness were synthesized by directly reacting $SbCl_3$ and $Na_2S_2O_3$ in the water, without any organics used in the experiment. Comprehensive structural investigations including XRD, ED, and HREM show that the nanoribbons are pure orthorhombic phase Sb_2S_3 (JCPDS 42-1393). The nanoribbons grow along [001] direction. The growth mechanism of the nanoribbons was investigated based on the TEM observations. A UV−visible absorption spectrum reveals that the nanoribbons are a semiconductor with a band gap of about 1.5 eV, near to the optimum for photovoltaic conversion, which suggests that Sb_2S_3 nanoribbons may be very promising for applications in solar energy and photoelectronics.

Acknowledgment. The authors are grateful for the support of the Ministry of Science and Technology (973 Grant No. 001CB610502 and 863 Grant No. 2004AA302G11), the National Science Foundation of China (Grant No. 90206201 and 10434010), the Chinese Ministry of Education (Key project. Grant No. 10401), and the National Center for Nanosecience and Technology of China.

References and Notes

(1) Huang, Y.; Duan, X. F.; Cui, Y.; Lauhon, L. J.; Kim, K. H.; Lieber, C. M. *Science* **2001**, *294*, 1313.
(2) Bachtold, A.; Hadley, P.; Nakanishi, T.; Dekker, C. *Science* **2001**, *294*, 1317.
(3) Martel, R.; Schmidt, T.; Shea, H. R.; Hertel, T.; Avouris, P. *Appl. Phys. Lett.* **1998**, *73*, 2447.
(4) Hofmann, W. *Z. Kristallogr.* **1933**, *86*, 225.
(5) Scavnicar, S. *Z. Kristallogr.* **1960**, *114*, 49.
(6) Roy, B.; Chakbraborty, B. R.; Bhattacharya, R.; Dutta, A. K. *Solid State Commun.* **1978**, *25*, 937.
(7) Savadogo, O.; Mandal, K. C. *Sol. Energy Mater. Sol. Cells* **1992**, *26*, 117.
(8) Abrikosov, N. K.; Bankina, V. F.; Poretakaya, L. V.; Shelimova, L. E.; Skudnova, E. V. In *Semiconducting II-VI and V-VI Compounds*; Tybulewicz, A., Ed.; Plenum: New York, 1969; p 186.
(9) Arivuoli, D.; Gnanam, F. D.; Ramasamy, P. *J. Mater. Sci. Lett.* **1988**, *7*, 711.
(10) Goryunova, N. A.; Kolomiets, B. T.; Malkova, A. A. *Sov. Phys. Technol. Phys.* **1956**, *1*, 1583.
(11) Karpus, A. S.; Batarunas, I. V.; Mikalkevichus, M. P. *Liet. Fiz. Rinkinys* **1962**, *2*, 289.
(12) Ibuke, S.; Yochimatsu, S. *J. Phys. Soc. Jpn.* **1955**, *10*, 549.
(13) Bube, R. *J. Appl. Phys.* **1960**, *31*, 315.
(14) Audzionis, A. I.; Batarunas, I. V.; Karpus, A. S.; Kudzhmauskas, Sh. L. *Liet. Fiz. Rinkinys* **1965**, *5*, 481.
(15) Zheng, X. W.; Xie, Y.; Zhu, L. Y.; Jiang, X. C.; Jia, Y. B.; Song, W. H.; Sun, Y. P. *Inorg. Chem.* **2002**, *41*, 455.
(16) Arun, P.; Vedeshwar, A. G. *J. Appl. Phys.* **1996**, *79*, 4029.
(17) Lokhande, C. D. *Mater. Chem. Phys.* **1991**, *27*, 1.
(18) Engelken, R. D.; Ali, S.; Chang, L. N.; Brinkley, C.; Turner, K.; Hester, C. *Mater. Lett.* **1990**, *10*, 264.
(19) Yang, J.; Zeng, J. H.; Yu, S. H.; Yang, L.; Zhang, Y. H.; Qian, Y. T. *Chem. Mater.* **2000**, *12*, 2924.
(20) Wang, H.; Zhu, J. J.; Chen, H. Y. *Chem. Lett.* **2002**, *12*, 1242.
(21) Wang, J. W.; Li, Y. D. *Mater. Chem. Phys.* **2004**, *87*, 420.
(22) Jiang, Y.; Zhu, Y. J. *J. Phys. Chem. B* **2005**, *109*, 4361.
(23) Yang, J.; Liu, Y. C.; Lin, H. M.; Chen, C. C. *Adv. Mater.* **2004**, *16*, 713.
(24) Pan, Z. W.; Dai, Z. R.; Wang, Z. L. *Science* **2001**, *291*, 1947.
(25) Wang, Z. L.; Pan, Z. W. *Adv. Mater.* **2002**, *14*, 1029.
(26) Comini, E.; Faglia, G.; Sberveglieri, G.; Pan, Z. W.; Wang, Z. L. *Appl. Phys. Lett.* **2002**, *81*, 1869.
(27) Mo, M. S.; Zeng, J. H.; Liu, X. M.; Yu, W. C.; Zhang, S. Y.; Qian, Y. T. *Adv. Mater.* **2002**, *14*, 1658.
(28) Liu, Z. P.; Peng, S.; Xie, Q.; Hu, Z. K.; Yang, Y.; Zhang, S. Y.; Qian, Y. T. *Adv. Mater.* **2003**, *15*, 936.
(29) Wang, R. H.; Chen, Q.; Wang, B. L.; Zhang, S.; Peng, L.-M. *Appl. Phys. Lett.* **2005**, *86*, 133101.